Full Length Article

Combined analytical strategies for chemical and physical characterization of tar from torrefaction of olive stone

Anna Trubetskaya [a,*], Robert Johnson [b], Rory F.D. Monaghan [c,d], Andrezza S. Ramos [e], Anders Brunsvik [f], Bernd Wittgens [f], Yinglei Han [g], Italo Pisano [a], James J. Leahy [a], Vitaliy Budarin [h]

[a] Department of Chemical Sciences, University of Limerick, Limerick, Ireland
[b] Arigna Fuels, Arigna Carrick-on-Shannon Co. Roscommon, Ireland
[c] School of Engineering and Ryan Institute, National University of Ireland Galway, Galway, Ireland
[d] MaREI, the SFI Research Centre for Energy, Climate and Marine, Galway, Ireland
[e] Departamento de Química, Universidade Federal do Amazonas, 69077 Manaus, Brazil
[f] SINTEF Industry, Richard Birkelands vei 2B, 7034 Trondheim, Norway
[g] Department of Biological Systems Engineering, Washington State University, Pullman, WA 99164, USA
[h] Department of Chemistry, The University of York, Heslington, York YO10 5DD, UK

ARTICLE INFO

ABSTRACT

The advance in analytical methodology is critical for progress in 1) biorefinery and 2) torrefaction product commercialization. The chemical characterisation of torrefaction liquid and concentrated tar produced by Arigna Fuels' pyrolysis plant allowed identification of polar, volatile, non-volatile compounds, species containing organically bound sulphur and nitrogen heteroatoms. The results suggest that only combined use of ion chromatography with Fourier Transform Ion Cyclotron Resonance Mass Spectrometry, and ^{1}H-^{13}C HS-QC can provide comprehensive information on sugar-like material and lignin-derived compounds. Due to the technical robustness and short analysis time, Fourier Transform Ion Cyclotron Resonance Mass Spectrometer was found to be a promising tool for tar analysis containing heavy molecular compounds. Importantly from a technological standpoint, the presence of aromatic and saturated compounds in both liquid and concentrated tar samples indicated the predominance of lignin-derived compounds over products originating from cellulose and hemicellulose polymers.

1. Introduction

Increasing human population and global warming require the development of new sustainable, environmental-friendly and cost efficient technologies for energy conversion. Torrefaction is a mild pyrolysis process that converts biomass into a carbon enriched material with high energy density and decreased oxygen content. Conversion of olive residues to value-added products via torrefaction can provide a potential solution to solid waste problems, while the liquid tar by-product can provide a valuable source of green carbon for the chemical, metallurgical and construction industries [1–3]. Recently, tar product has been defined as all the hydrocarbons with a molecular weight higher than benzene [4]. Compositional studies on liquid tar by-products have resulted in several research papers in recent years. Knowledge of the

composition of liquid tar by-product is important to better understand the torrefaction process as well as further refinement of value-added products.

The chemical structure of torrefaction tar possesses an analytical challenge to study. This is due to the presence of complex mixtures containing compounds of low and high polarity which are tendentious to resolve with conventional techniques [5]. During torrefaction, three different product groups are formed (1) concentrated char, (2) condensable volatile organic compounds comprising water, acetic acid, higher aldehydes, alcohols, and ketones, and (3) non-condensable gases such as CO_2, CO, and small amounts of methane [6]. The condensable liquid products can be further divided into four subgroups: (1) water generated as a by-product from biomass thermal decomposition, (2) freely bound water that has been released through evaporation, (3)
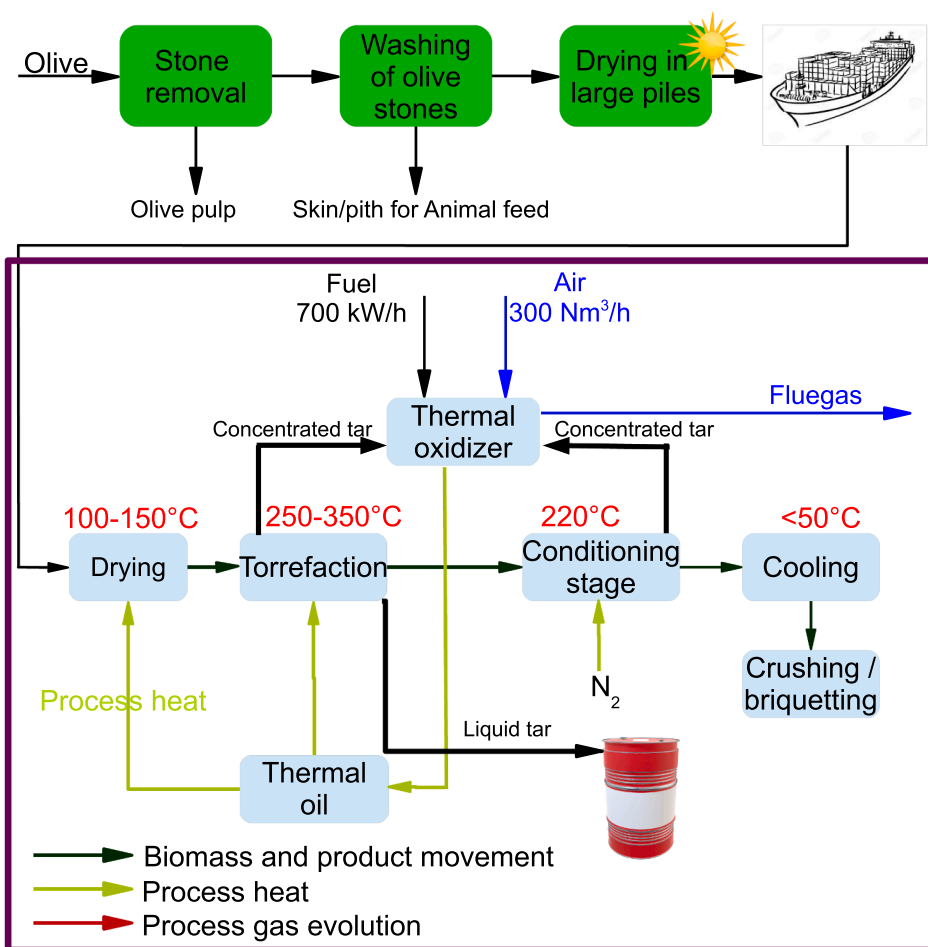

Fig. 1. Arigna torrefaction plant combined with the destoning of olives schematic.

polar organic species e.g. acetic acid, methanol, furfural, methoxy-phenols and fatty acids, and (4) lipids, which contain higher molecular weight compounds such as waxes [7]. Literature defines the liquid tar as an organic product that contains all four subgroups [8]. During biomass torrefaction, evolved gaseous tars can condense on the walls of exhaust pipes leading to gas-line blockages and formation of concentrated tar products [9]. Acetic acid is a major product in the liquid fraction that originates from acetoxy- and methoxy-groups present as side chains in xylose units [10]. In addition, small quantities of formic acid, lactic acid, furfural, hydroxyl acetone, and traces of phenol were detected in the condensed liquid sample [11].

Many attempts are being made to characterise physicochemical properties of pyrolysis liquid products [12]. However, the inherent complexity of the liquid products from biomass torrefaction hinders a full identification of their constituents. Literature reports that torrefaction of *Pubescens* at 200 °C generated liquid tar samples with compound molecular weights varying from 200 to 2000 Da using gel permeation chromatography techniques [13]. Reversed-phase liquid chromatography (LC) with UV detector indicated that coal/ biomass tar might contain large PAHs with more than 7-rings [14]. This indicates that compositional analysis of the torrefaction tar requires the development of methods for preparation, introduction and ionization of low and heavy molecular fractions [15]. Literature sources also reported that analytical techniques for bio-oil characterisation can be classified in (1) GC–MS detectable volatile compounds, (2) total carbohydrates (slightly dehydrated sugars and furans), (3) phenols, (4) highly dehydrated structures rich in carbonyl groups, and (5) carboxylic groups [16].

The accuracy of tar characterisation using chromatographic methods only is limited because only a small fraction of the molecular-weight distribution can be analysed [17]. The reassignment of carbohydrates and methoxy/hydroxy regions during ^{13}C NMR analysis of tar samples can hinder functional group assignment of the cellulosic component, leading to challenges in the distinction between aromatic and carbohydrate products [18]. Although the phenol content significantly varies in tar samples depending on the method used, only a small fraction (less than 10%) is shown in the form of GC–MS detectable phenols [19]. This indicates that most of these phenols are condensation reaction products in the form of high molecular weight compounds [16]. Moreover, the efficiency of electron ionization using various spectroscopic techniques for tar structure characterisation increases with the size of the molecule [20]. High resolution Fourier Transform Ion Cyclotron Resonance Mass Spectroscopy (FT-ICR MS) can be used to characterise tar structure with respect to molecular weight distribution, exact masses, chemical formulas and isoabundance plots [21–25]. Compared to MALDI-TOF platforms, FT-ICR has a better resolution in a similar detection range [26–28].

In the present study, an approach for the detailed componential characterisation of torrefaction tar has been shown for the first time. The aim of this study was to evaluate the chemical composition of torrefaction tar using FT-ICR MS, two-dimensional ^{1}H-^{13}C HS-QC NMR, headspace gas chromatography-mass spectrometry (HSGC-MS), GC-FID, MS, UV-Fluorescence and ESI. In addition, the two-dimensional ^{1}H-^{13}C HS-QC was conducted for both liquid and concentrated tar samples to determine differences in their chemical composition. Torrefaction tar viscosity was characterised using a rheometer. The differences in physicochemical properties of torrefaction tar were correlated to the kinetics derived from thermogravimetric analysis.

2. Materials and methods

2.1. Raw materials

Washed olive pits (Olea europaea) were sourced from the Mediterranean region and are a by-product of the olive oil industry where they are separated, crushed to < 3 mm and air dried. Figure 1 illustrates the biomass torrefaction and briquetting processes at Arigna Fuels combined with olive destoning offsite. Prior to olive oil extraction, stones are removed from the olive fruit, washed to provide skin and pith for animal feed and later dried in large piles [29]. The torrefaction of olive stones was carried out at 280 °C during a 24 h long production [30]. The dryer and pyrolysis reactors are both heated indirectly with thermal oil. Liquefied petroleum gas (LPG) is used to heat the plant initially and start the torrefaction process, but when gases are produced, these are combusted in a thermal oxidizer to provide heat to the drying and torrefaction processes and no further heat source is required. The heat recovered from thermal oil is used for the drying of coal briquettes produced at the integrated coal briquetting plant. The torrefied biomass is cooled to room temperature, further crushed and briquetted. Liquid tar was collected from an opening located in the exhaust pipe during torrefaction and stored at ambient temperature in a desiccator. The pipe temperature and sampling port is maintained at 220 °C to prevent condensation of any organic matter. Volatiles emitted during torrefaction can condense on reactor walls forming a viscous tar product leading to blocked pipes between the torrefaction unit, thermal oxidizer and conditioning stage. The concentrated tar sample was collected from the thermal oxidiser feed pipes, following completion and cooling (< 50 °C) of the torrefaction process due to a safety precaution.

2.2. Characterisation techniques for liquid and concentrated tar analysis

2.2.1. Elemental analysis

A Leco TruSpec CHN 628 series instrument was used to analyse the tar samples for carbon, hydrogen, and nitrogen content following ASTM D5373-08. The oxygen content was calculated by difference. 0.15 g of the oil sample was weighed into a tin foil cup, and then approximately 0.3 g of Leco's Com-Aid was added on top and the foil cup was sealed by hand. Three-point calibrations were completed using LECO 502–092 EDTA.

2.2.2. Lignocellulosic analysis

The samples were hydrolysed to determine structural carbohydrates and lignin in tar samples [31]. The process includes two main steps: 1) two-stage acid hydrolysis; 2) separation of the hydrolysate from the acid insoluble residue (AIR) through gravimetric filtration. Klason lignin (KL) was determined by measuring the weight difference between the AIR and the ash content. Acid soluble lignin (ASL) was determined by absorbance of the hydrolysate at 205 nm. The 8453 UV–vis spectrophotometer (Agilent, USA) was used to determine the absorbance which was converted to concentration using Beer's law [31]. ICS-3000 AS50 ion chromatography (Dionex, USA) was used to determine the lignocellulosic sugars obtained after hydrolysis. 10 µl of the diluted sample was injected to achieve sugar separation into arabinose, rhamnose, galactose, glucose, xylose, and mannose. The analysis consisted of diluting the hydrolysate samples 20x with a deionised water solution containing known amounts of internal standard (melibiose). Deionised water was used as the eluent; the flow rate applied was 1.5 mL min^{-1}, and the column/detector temperature was 21 °C. Furthermore, NaOH (300 mM) was added to the post-column eluent stream due to the photodiode array detector requiring an alkaline environment in order to detect the presence of carbohydrates. NaOH was added using a Dionex GP40 pump, at a flow rate of 0.3 mL min^{-1}.

2.2.3. Thermogravimetric analysis

Moisture, fixed carbon, volatiles, and ash content of the liquid tar sample were determined using a thermo-gravimetric analyser (TGA) SDTA851e (Mettler Toledo, US). Briefly, moisture content was measured as the weight loss after the tar was heated in a crucible from 25 to 120 °C and held at this temperature for 3 min under nitrogen gas at a flow rate of 50 ml min^{-1}. The tar sample was then heated from 120 to 950 °C under nitrogen gas to determine the volatile content, following which it was held for 5 min and later cooled to 450 °C. Ash was determined after heating the tar from 450 to 600 °C under flowing oxygen (50 ml min^{-1}). All measurements were conducted in duplicate to establish sufficient reproducibility.

2.2.4. Qualitative ^1H-^{13}C heteronuclear single quantum coherence analysis

Samples of around 30.2 mg were dissolved in 550 µl of chloroform or acetone (0.05% TMS). Heteronuclear single quantum coherence (HS-QC) spectra (^1H at 500.13 MHz and ^{13}C at 125.7 MHz) were recorded at 25 °C on a Bruker Avance III HD 400 MHz instrument equipped with TopSpin 2.1 software. The pulse sequences zgpr were used to suppress the residual water signal. ^1H-^{13}C HS-QC spectra were obtained applying the following parameters for acquisition: TD (F2 and F1) = 2048 and 256 Hz. The Bruker COSY pulse program in DQD acquisition mode was used, with NS = 64; TD (F2 and F1) = 2048 and 256 Hz; SW (F2 and F1) = 129836 ppm and 215 ppm; O2 (F2) = 12575.78 Hz, O1 (F1) = 2749.02 Hz; D1 = 1.0 s; CNST2 (1 J(C–H) = 145; acquisition time F2 channel = 0.1576960 ms, F1 channel = 0.0047336 ms; pulse length of the 90° high power pulse P1 was optimized for each sample. The Bruker Cosy pulse program in DQD acquisition mode was used, with NS = 32; TD (F2 and F1) = 2048 and 128 Hz; DS = 8; SW (F2 and F1) = 13.0627 ppm; O1 (F2 and F1) = 2768.55 Hz.

2.3. Characterisation techniques for liquid tar analysis

2.3.1. Solubility

Liquid tar was dissolved in 8 different solvents obtained from Merck and Fluka with > 99% purity. 1 g of tar and 20 ml solvent were added to a vial which was placed in an ultrasonic bath for 2 h. Afterwards, the solution was filtered using a PTFE filter with a pore size of 0.45 µm under vacuum and the residue was washed until the filtrate became totally clear. The residue was dried to constant weight, as reported in Guillen et al. [32].

2.3.2. UV-Fluorescence (synchronized)

Liquid tar was diluted in HPLC grade methanol to 100 ppm and analysed on a Shimadzu RF 5301 pc (software: Panorama Fluorescence 2.1) spectrometer. Synchronous fluorescence spectra at constant wavelength difference were set. The excitation wavelength was scanned from 250 to 700 nm, and emission wavelengths were recorded at 15 nm intervals (from 265 to 715 nm). The excitation slit width and emission slit width were set at 3 nm. Data was collected every 1 nm.

2.3.3. KF titration

Water content of the sample was determined by Karl Fischer titration as per ASTM E203-08 (Standard Test Method for Water Using Volumetric Karl Fischer Titration) using a Schott Instruments TitroLine Karl Fischer volumetric titrator. Deionized water (> 18.18 MΩ cm) was used for calibration.

2.3.4. Fourier transform ion cyclotron resonance mass spectrometer

10 mg of tar sample was dissolved in 990 µl of tetrahydrofuran. Prior to FT-ICR analysis, a 1.5 ml aliquot was pipetted into the autosampler screw cap vial. Mass spectra were acquired using a Bruker solari XRFourier transform ion cyclotron resonance mass spectrometer (Bruker Daltonik GmbH, Germany) equipped with a 12 T refrigerated actively-shielded superconducting magnet (Bruker Biospin, France) and the new dynamically harmonized analyser ParaCell (Bruker Daltonics GmbH, Germany). The mass range was set to m/z 150–4000 using 4 M data points with a transient length of 1.6 s resulting in a resolving power

Table 1

Proximate and ultimate analysis of raw olive stones, liquid and concentrated tar.

	Moisture	Ash	Volatiles	C	H	N	O	HHV
	%, as received			%, dry basis				MJ kg^{-1}
Olive stones	15.5	0.8	76	44.8	5.8	0.2	48.3	20.3
Liquid tar	5.4a	1.1	89	64.2	6.7	0.1	29	26.1
Concentrated tar	0.8[a]	0.4	36.6	72.7	5.5	0.9	20.9	29.3

[a] Moisture in the tar was determined using Karl Fisher titration. The moisture content was subtracted from the hydrogen and oxygen content of the liquid tar to show the elemental analysis data in % on dry basis.

of 450000 at m/z 400 in magnitude mode. A linear calibration was applied. The root mass square (RMS) mass error of the recalibration of all acquired spectra was better than 150 ppb using a linear calibration. The molecular formula calculation was performed in Composer 1.0.6 (Sierra Analytics, USA) using a maximum formula of $C_nH_hN_3O_3S_3$. The relative abundances of the compound classes were calculated with Composer software. Statistical analysis was performed with the software ProfileAnalysis 2.1 (Bruker Daltonics GmbH, Germany). Carbon number and double bond equivalence (DBE) number were determined for each mass peak, using equation 1 [33]:

$$DBE = C - (H/2) + (N/2) + 1 \qquad (1)$$

2.3.5. Electrospray ionization mass spectrometry

5 mg of liquid tar was dissolved in methanol containing 1% acetic acid (2 ml) and directly analysed in both positive and negative ion electrospray ionization-mass spectrometry (ESI-MS, m/z 90–2000) on a Finnigan LCQ-Deca instrument (Thermoquest, USA) at a flow rate of 10 µl min^{-1}. Data analysis was based on the calculation of number average molar mass (M_n) as $M_n = \sum M_iN_i / \sum N_i$ and the weight average molar mass (M_w) as $M_w = \sum M_i^2 N_i / \sum M_i N_i$ with M_i as m/z and N_i as intensity of ions [34].

2.3.6. Headspace gas chromatography-mass spectroscopy

Approximately 20 mg of a liquid tar was accurately weighed and directly sealed into a 20 ml headspace vial. Headspace gas chromatography-mass spectroscopy (HSGC-MS) analysis was performed using an Agilent 7694E Headspace sampler (Agilent Technologies, Germany), connected to an Agilent 7890B series gas chromatograph (Agilent Technologies, Germany) coupled with an Agilent 5977A series mass spectrometer (Agilent Technologies, Germany) and equipped with a HP-5MS Agilent column (0.25 mm x 30 m x 0.25 µm). The headspace operating conditions were as follows: the equilibration time was 20 min; the headspace oven, loop, and transfer line temperatures were 100, 120 and 150 °C, respectively; the vial was shaken for 2 min at low intensity; the injecting time was 2 min in an analysis cycle. GC operating conditions were as follows: carrier gas (helium) was set at a flow rate of 4.0125 ml min^{-1} with a split ratio of 10:1; the column temperature program was initially set at 80 °C for 2 min in an analysis cycle, and gradually increased to 325 °C at 15 °C min^{-1}, then kept for 5 min. For MS detection, an electron ionization (EI) system was used with ionization energy at 70 eV; temperatures of the ion source and quadrupole were 230 and 150 °C, respectively; the mass range was 50–550 amu in full-scan acquisition mode with 3 min of solvent delay. The HSGC-MS collected data were processed by MassHunter Qualitative Analysis B.06.00 for peak deconvolution. The mass spectra with well-resolved peaks were imported into the mass spectra library software NIST MS Search 2.3 [35].

2.3.7. Rheometer

The stored deformation energy (G') of the tar sample was measured in pascals (Pa) using a Discovery Hybrid Rheometer-2 (TA Instruments, Ireland), as reported in previous studies [36]. This instrument is equipped with a heating unit that maintains the sample from 30 to 150 °C, with a stainless-steel cone and disposable parallel aluminium plates.

Table 2

Lignocellulosic and ash composition of liquid and concentrated tar samples, calculated in percentage (wt.% dry basis).

Sample	Glucose	Lignin		Extractives	Ash
		acid insoluble	acid soluble		
Liquid tar	0.4	3.4	0.1	96.3	1.1
Concentrated tar	0.2	58.7	0.7	40.9	0.4

The cone has an angle of 48 degrees and both, cone and plate have a diameter of 25 mm.

3. Results

3.1. Liquid and concentrated tar characterisation

3.1.1. Elemental analysis

Proximate and ultimate analysis of raw olive stones and liquid/ concentrated tar samples are shown in Table 1. The moisture content in the liquid tar was low due to the torrefaction temperature of 280 °C, where mostly low molecular weight compounds were formed [16]. The concentrated tar showed low oxygen contents and thus, relatively higher calorific value than the liquid tar [37]. In addition, the high heating value of the concentrated tar is like that of bio-oil from fast pyrolysis and liquid tar from torrefaction in the range of prepared in the range of 240 to 300 °C [16,38]. The low ash content showed that both concentrated and liquid tar samples mostly consist of organic compounds.

3.1.2. Lignocellulosic analysis

The liquid and concentrated tar overall contained only traces of sugars varying from 0.2 to 0.4 wt.% on dry basis, as shown in Table 2. Pyrolytic sugars typically contribute to 5–10 wt.% of bio-oil from biomass pyrolysis in the range 400–600 °C [39]. The results of the present study have shown that only glucose was present in both tar samples. Small traces of sugars in tar samples likely originate from the pyrolysis of cellulose compounds in raw olive stones. This indicates that the remaining compounds in tar samples are largely composed of pyrolytic lignin macromolecules and compounds derived from it, as previously suggested [40]. These results are comparable with findings using FT-ICR instrumentation (Section 3.3.3) whereas heteroatom class distribution and double bond equivalence showed composition of the liquid tar consisted of distinguished phenols derived from lignin. In addition, a large fraction of extractives was found in tar samples. These might be proteins, polymerized compounds, uronic acids, acetyl acids, etc. [41,42]. The higher lignin content in the concentrated tar indicates a more stable molecular structure than that of liquid tar, confirming previous results of Yu et al. [43].

3.1.3. Thermogravimetric analysis

Figure 2 shows differential weight loss curves (DTG) for oxidation (5% by volume) of liquid and concentrated tar samples. The DTG curve of concentrated tar shows a triple peak at 315, 400 and 610 °C, whereas the DTG curve of liquid tar shows a double broad peak at 190 and
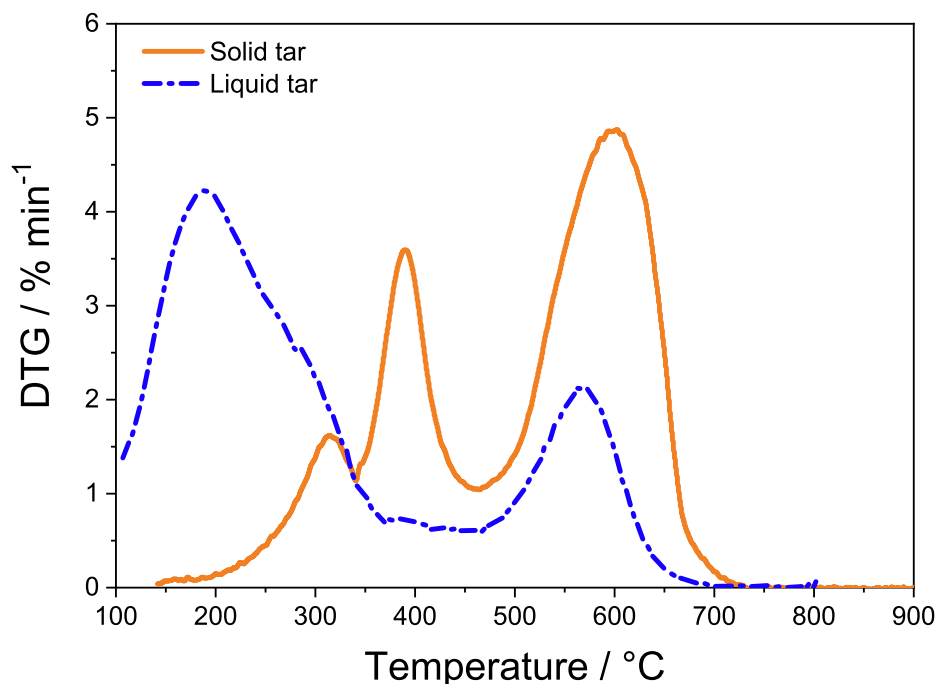
Fig. 2. DTG curves of liquid tar and concentrated tar reacted in 5% volume fraction O_2 + 95% volume fraction N_2.
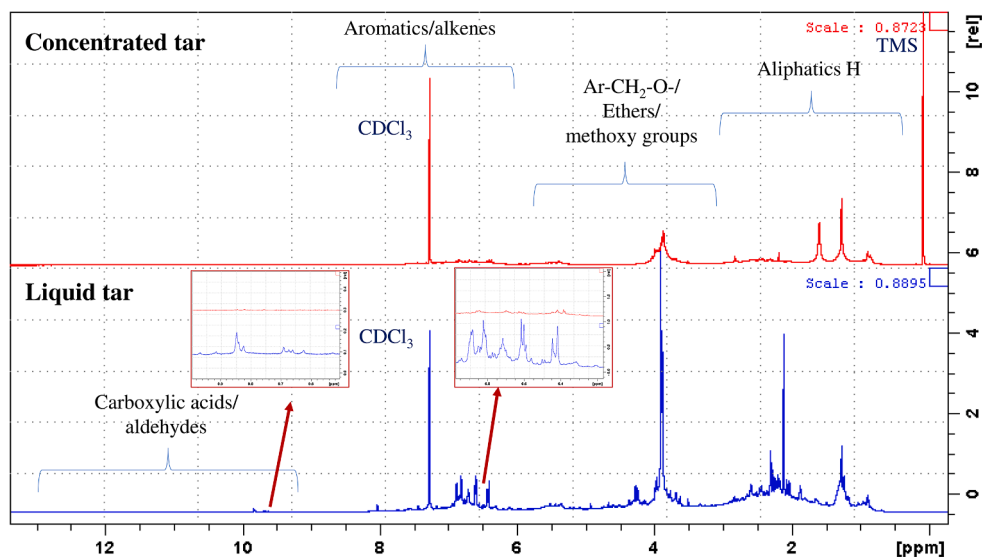

Fig. 3. Comparison of ^{1}H NMR spectra of the liquid and concentrated tar samples dissolved in chloroform using 600 MHz.

575 °C, both of which indicate a heterogeneous tar mixture with respect to O_2 reactivity. Decomposition of volatile compounds in the liquid tar occurs in the temperature range from 60 to 375 °C with the peak temperature at 190 °C attributed to devolatilization of light volatile compounds. The decomposition rate of concentrated tar was shifted to higher temperatures from 150 to 460 °C with two significant peaks at temperatures of 315 and 400 °C, indicating devolatilization of light volatiles i.e. acids, aliphatic species, and alkylphenols at low temperatures and fewer oxygen-containing compounds of aromatic and polyaromatic origin in the range 350 to 460 °C [44,45]. The peak DTG temperature of concentrated tar is shifted to higher temperatures than that of liquid tar. Presence of oxygenated aromatics in the liquid tar is known to increase the reaction rate [46]. The cross-linked polyaromatic structure of concentrated tar with more carbon and less hydrogen than in liquid tar could decrease the oxidation reactivity [47]. (See Figure 3).

3.1.4. ^{1}H-^{13}C NMR measurements

Differences in solubility between the liquid and concentrated tar samples were observed, whereas the liquid tar sample showed greater chemical information in signals compared to the concentrated tar. Based on HSQC, HMBC and COSY analysis it was possible to identify the chemical shift ranges of functional groups of different chemical structures. In the ^{13}C NMR experiments about 166 signals from the different major molecules were observed in the liquid tar, while only 21 signals were seen in the concentrated tar. The chemical shifts of compounds present in torrefaction products are summarized in the Supplemental material (Table S-1). The more intense signals at 56, 106.5, 107, 116, 119, 120, and 172 ppm were associated with the presence of carbon species which originate from lignin [48]. The less soluble concentrated tar sample showed mostly aliphatic C–C signals, whereas the liquid tar contained aromatic and aliphatic carbon nuclei.

On both samples a large amount of residual unbranched carbon skeleton (peaks at 56 ppm) was observed corresponding to methyl and aliphatic groups from fatty acids such as hexadecenoic acid (C16), oleic acid (C18:1) and linoleic acid (18:2) as described by HSGC-MS [49]. In comparison to the concentrated tar, ^{1}H NMR analysis of the liquid tar sample showed greater concentrations of aromatic and conjugated alkene hydrogen contents (8.2–6.0 ppm) [50]. Overall, the ^{1}H NMR analysis showed that aliphatic protons are more prevalent than protons which are proximal to heteroatoms (alcohols, carbohydrates) in both liquid and concentrated tar samples. The most upfield region 28–0 ppm indicated the presence of methyl groups and the region 50 to 28 ppm contains a high percentage of aliphatic carbons which are most likely methylene carbons (CH_2) which are associated with longer aliphatic chains [51]. The region 95–50 ppm in the ^{13}C NMR spectra represents carbon atoms which are adjacent to an O atom in carbohydrates, ethers, or alcohols.

Predictably, the relative amount of these types of carbon atoms follows the same general trend as their overall oxygen content with higher oxygen content in the liquid tar than in the concentrated tar sample. In addition, the region between 95–50 ppm indicated that the liquid tar contains significantly fewer carbohydrates and aliphatic compounds with OH groups than the bio-oil generated from herbaceous feedstocks, as reported by Mullen et al. [17]. Compared to bio-oil obtained from fast pyrolysis of herbaceous feedstocks and chicken litter, torrefaction tar was assumed to derive mostly from lignocellulosic monomers, rather than from aliphatic branching, as shown in the Supplemental material (Fig. S-3(a)).

3.2. Liquid tar characterisation

3.2.1. Tar solubility

Solubility tests were carried out to determine a suitable solvent to dissolve and disperse the tar used for the experimental runs with various analytical techniques. Table 3 shows that the liquid tar was most soluble in 1-methyl-2-pyrrolidinone (86.9 wt.%) and dimethyl sulfoxide (90.8 wt.%). It is worth pointing out that the reproducibility of the extraction experiment is not identical for all solvents. NMP and DMSO solvents give more reproducible extraction yields than C_2H_5OH, ACN and other solvents, confirming the previous results of Guillen et al. [32].

3.2.2. UV-fluorescence

The fluorescence emission bands at 274, 315, 325 and 350 nm were detected in the liquid tar sample which were attributed to higher molecular weight aromatics because of increased conjugation during torrefaction, as shown in the Supplemental material (Fig. S-8) [52,53]. The multiaromatic and conjugated ring systems indicate that only two- to a maximum of four-ring aromatic systems are present in the liquid tar from olive stone torrefaction, confirming the previous results of Stankovikj et al. [16]. This is indicated by the presence of absorption bands in the region of 500 to 700 nm. The intensity of the UV-Fluorescence spectra decreased with increasing molecular size and with increasing sizes of polycyclic aromatic (PCA) units embedded within large molecules in the torrefaction tar. The effects were explained by the transfer of intramolecular energy within large molecules which diminish fluorescence quantum yields for larger PCA units [54,55]. Thus, the method has limitations in estimation of molecular weights of heavy tar fractions.

3.2.3. Direct injection gas chromatography-mass spectrometry

GC–MS analysis of the liquid tar was conducted and the chromatogram with compounds identified is shown in the Supplemental material (Fig. S-9 and Table S-2) respectively. A match quality of > 85% was accepted for the identification of the compounds and the MS signatures were visually compared with the database entries for best match. Qualitative analysis of the liquid tar identified phenols and their derivatives, benzenoids, phenethylamine, and imidazoles, which were previously found in the GC–MS analysis of lignocellulosic compounds [56,57]. The present GC–MS results correspond to the compounds found in the HSGC-MS analysis, as discussed in section 3.3. However, the present GC–MS results indicated that the liquid tar mostly consists of detectable volatile compounds while the heavy molecular weight fractions were not detectable using this method.
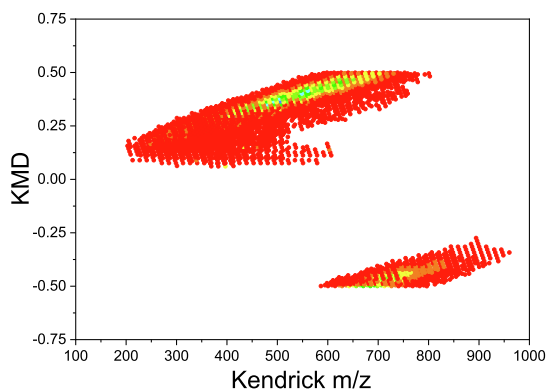
3.3. HSGC-MS

Formation of the main compounds in liquid tar was investigated by HSGC-MS with more than 100 peaks detected. The major target compounds with a spectral match quality greater than 85% are listed in the Supplemental material (Table S-3). The results show that compounds formed during torrefaction are all oxygenated species, arising from the large amount of oxygen in lignocellulose. The main products of the HSGC-MS analysis of the liquid tar were vanillin, cresols, dihydroeugenol, methoxy- eugenol, *trans*-isoeugenol and guaiacol forming the non-condensed structure of lignin in the feedstocks. In addition, the presence of *p*-cresol in the tar is due to high abundance of methoxy groups in olive stones which are rich in guaiacyl and p-hydroxyphenol units indicating that the lignin structure of olive stones is similar to that of hardwood [58]. The presence of *O*-guaiacol, vanillin and dihydroeugenol in the olive stone tar indicated that the chemical structure of tar is like that of monomers in the raw lignin.
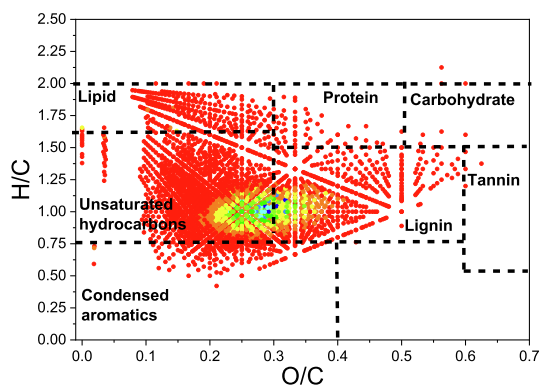
3.3.1. GC-FID

The analysis of fatty acid composition of liquid tar was carried out using a quantitative GC-FID method with the tridecanoic acid as an internal standard, as shown in the Supplemental material (Fig. S-10). The results showed that torrefaction tar from olive stones contains hexadecenoic acid (C16), oleic acid (C18:1) and linoleic acid (18:2). In addition, fatty acids are present in the liquid tar as it was observed during HSGC-MS analysis (Section 3.3). The raw olive stones contain a small amount of residual oil which generated the oxidation products in a form of acids.
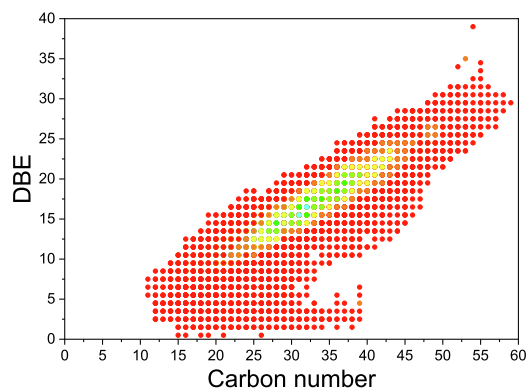
3.3.2. ESI-MS

The ESI-MS results indicate the presence of oligomers in liquid tar dissolved in methanol containing 1% acetic acid with negative and positive molecular ions shown in the Supplemental material (Figs. S-8a and S-8b), respectively [16,59,60]. Since most of the phenolics can be easily identified through negative ionization in the ESI, this method was selected to demonstrate the molecular distribution of the tar and then used to calculate the average molar mass (M_n and M_w). The number and weight average molar masses were 800 and 1000, respectively. The polydispersity index was then calculated to be 1.29. The main detected negative ions are listed in the Supplemental material (Table S-1) with their relative abundance presented as well. These ions ranged from 133.1 to 1984.52 (m/z) with smaller ions being mainly derived from substituted phenols, which were also identified by GC–MS, as seen in the Supplemental material (Fig. S-11).

Table 3

Liquid tar solubility using dimethyl sulfoxide (DMSO), tetrahydrofuran (THF), N-Methyl-2-pyrrolidone (NMP), acetone (C_3H_6O), chloroform ($CHCl_3$), methanol (CH_3OH), ethanol (C_2H_5OH), acetonitrile (ACN) in wt.% with standard deviation.

DMSO	THF	NMP	C_3H_6O	$CHCl_3$	CH_3OH	C_2H_5OH	ACN
90.8 ± 0.01	75.8 ± 0.04	86.9 ± 0.45	53.2 ± 0.56	60.5 ± 0.25	75.9 ± 0.24	66.3 ± 0.3	68.3 ± 0.45

(a): Kendrick plot (DMSO)
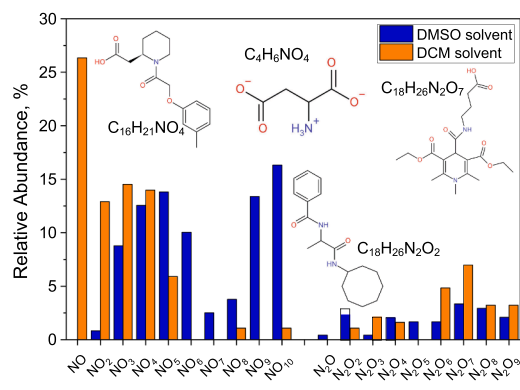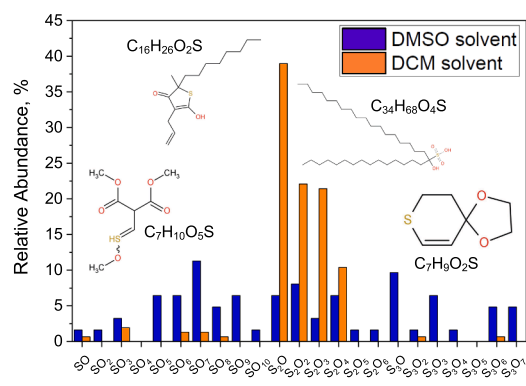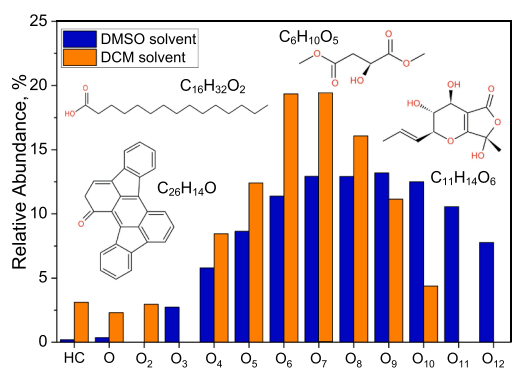

(b): Van Krevelen (DMSO)

(c): DBE over carbon (DMSO)

Fig. 4. (a)-(c) Contour plots of van Krevelen, Kendrick versus nominal mass, and DBE versus carbon number using DMSO as solvent for the liquid tar.

(a): N_xO_y distribution

(b): S_xO_y distribution

(c): O distribution

Fig. 5. (a)-(c) Heteroatoms N, S and O class distribution obtained via FT-ICR-MS analysis of the liquid tar.

3.3.3. FT-ICR MS

Figure 4 shows chemical composition analysis of the liquid tar using FT-ICR. The analysis procedure includes filtered liquid tar sample with DMSO as a solvent. Fourier transform ion cyclotron resonance mass spectrometry (FT-ICR MS) offers ultrahigh mass resolution and accuracy, which enables unique assignment of elemental compositions for thousands of fragments obtained from a single torrefaction tar sample. Overall, ESI FT-ICR MS covered a large chemical range up to m/z 950. The spectra of oxygen-rich compounds in the liquid tar were enhanced using DMSO as a solvent due to the presence of additional hydroxyl groups which increased deprotonation. Kendrick plot of the liquid tar showed a broad band with relatively high Kendrick mass defects. A significant fraction of compounds had lower Kendrick mass defects

forming a large cloud of points ranging over ΔKMD ≈ 0.375 (from 0.125 to 0.5) which represent large aliphatic species [5]. A narrow dense cloud of points ranging over ΔKMD ≈ 0.125 (from -0.5 to -0.375) represents the distribution of large aromatic compounds in the liquid tar [61–63].

Figure 5(c) shows that DMSO as a solvent gave a homogeneous distribution of oxygen atoms in oxygenated hydrocarbons in the range O_6-O_{10}. In addition to simply comparing the number of detected species, a van Krevelen diagram in Figure 4(b) was plotted to study the selectivity of FT-ICR MS analysis. The van Krevelen diagram is a widely applied graphical tool to study the evolution of fuels, arranging the molar ratio of hydrogen-to-carbon (H/C ratio) as ordinate and the molar oxygen-to-carbon ratio (O/C ratio) as abscissa. The dots drawn from the magnitude mode data exhibited gaps in the plot, and the chemical

composition was not distributed continuously, especially for species with low carbon numbers, because the mass resolving power of the FT-ICR MS was not sufficient to resolve the peaks of species which are present in a high concentration at higher m/z [64]. Some of the neighbouring peaks could merge or form complex polyaromatic structures; thus, it was possible to identify only one of the reacting compounds in the magnitude mode spectrum [65]. The dots generated for very high m/z, in contrast, exhibited a more continuous pattern. The average H/C and O/C ratios were approaching the ratios of unsaturated hydrocarbons, condensed aromatics, lignin and lipids samples during FT-ICR MS analysis. The van Krevelen diagram clearly shows that many more lignin-like compounds (O/C 0.2–0.6 and H/C 0.7–1.5) were detected via FT-ICR MS, confirming the previous results [66,67]. Figure 4(c) showed the DBE distribution (the degree of unsaturation) of each oxygen heteroatom class over the number of carbons. Compositional information (C_{55}; DBE = 30) in the DBE distribution graph 4(c) can be interpreted that the compound has 55 carbon atoms with 30 unsatured bonds. For the liquid tar, the total carbon and DBE numbers mainly range from 10 to 60 and from 1 to 32.5, respectively. This is also in line with the suggestion that the degree of unsaturation rapidly increases with the carbon number and molecular weight [68,69]. Single-ring aromatic compounds (DBE < 5) were abundant, followed by double-ring aromatic compounds (DBE 8–16) followed by large polyaromatic structures (DBE 16–35) with the same degree of unsaturation but different aliphatic side chains i.e. dibenzo[a,j]coronene [70,33]. Since the DBE values of benzene and naphthalene are 4 and 7, compounds detected in the present study were associated with (poly) aromatics [71,72]. Such conjugated π-systems can readily redistribute vibrational energy over the entire system and stabilize their core structures [73].

In addition, nitrogen-containing compounds ranging from N to N_2 were detected in liquid tar, leading to the broad DBE distributions ranging from 1 to 35, as shown in Figure 5(a). The C_n and DBE distribution indicated that liquid tar may include oxygenated derivatives of pyrrole, pyridine, indole, imidazole or pyrazine, corresponding to the results of GC–MS analysis, see section 3.2.3 and previous results [37]. The organic-nitrogen species found in liquid tar were mainly products from pyrolysis of proteins, lipids and polysaccharides in olive stones [74]. The presence of N_xO_y species in liquid tar showed at degree of

unsaturation like that of crude oil (DBE = 1–30), whereas the DBE values of biocrude from hydrothermal liquefaction and shale oil were below 17, as reported in previous studies [75–77]. In addition, both FT-ICR and elemental analysis presented in Table 1 report traces of non-aromatic nitrogen-containing species in the tar sample, confirming previous results [78,72]. Detected S_zO_x class compounds are most likely sulfonic acids or their derivatives, as shown in Figure 5(b). About 20–35% of sulphur content of the initial feedstock concentration can be released during wood pyrolysis and this release increases to 40–70% for herbaceous feedstocks in the range of 200 to 350 °C [79]. Previous torrefaction studies have indicated that the release of sulphur at 200–400 °C could originate from the decomposition of organically associated sulphur in the proteins [80,81]. However, no loss of sulphur was observed during the torrefaction process. In fact, on a wt.% basis it increases as per the inorganic species.

Figure 5(c) shows the distribution of compounds which were assigned to O_n class species with double bond equivalent (DBE) values of 1–35. The O_2-O_4 compounds represented by m/z 117, 137 and 151 were detected in low concentrations. The O_2 class compounds may be composed of hexadecanoic acid and octadecanoic acid [82]. The O_4 and O_5 class compounds were associated with the presence of aliphatics [83]. Thus, these compounds can be associated with both polyhydroxylcyclic hydrocarbons of cellulose and "phenolic compounds" of lignin. In addition, the O_6 compounds representing most of the lignin trimers were present in large quantities.

The O_5-O_8 exhibited high intensities in the mass spectrum and were associated with the "sugaric" components coupled to the nitrogen-containing species or with the phenolic compounds containing a carboxylic group [84,85]. The main compounds containing O_5-O_8 were likely cellulose-, hemicellulose-, lignin-derived depolymerization products, e.g., di- and trilignols which included two phenyl groups (C_n = 20–30; DBE > 8) [86]. Lipids i.e. fatty and amino acids and extractives i. e. resin acids, terpenes contain O_5-O_7 class compounds with C_n ranging from 20 to 25 [87]. Previous studies showed that lignin pyrolysis generated mainly monomers and dimers with a molecular mass centered around 400 Da [88]. The compounds detected in the O_9-O_{12} classes are likely to be phenolic extractives e.g., residues of quercetin with different glycosides based on the C_n and DBE values (C_n = 20–40; DBE = 11–19) [89,90].
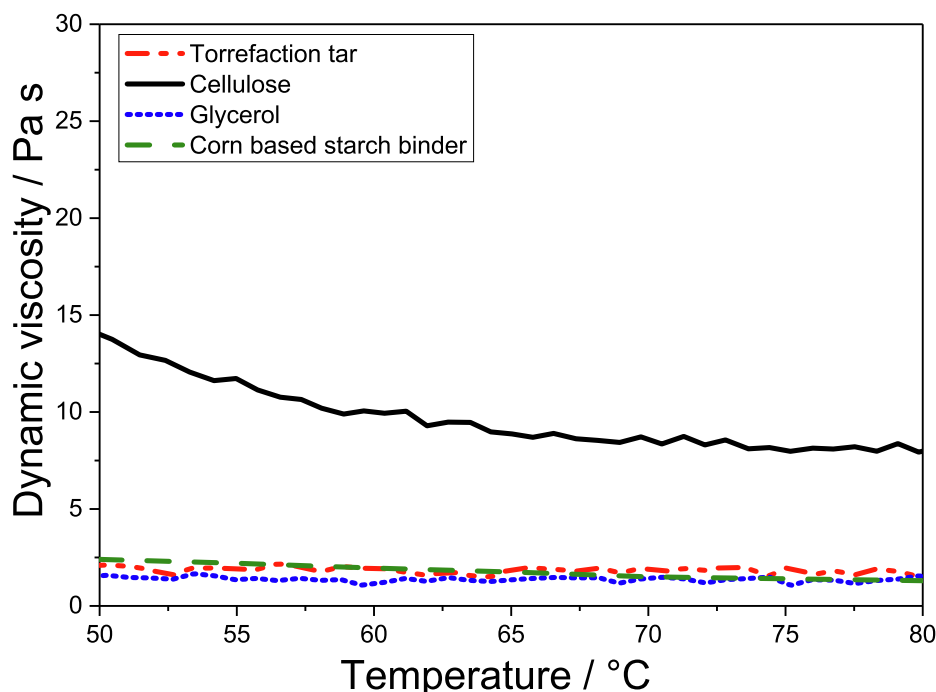

Fig. 6. Steady-state flow viscosity of the liquid torrefaction tar.

Table 4
Summary of the techniques used in the tar compositional analysis.

Technique	Solvent	Property	Classification	Highlights of tar analysis	Improvements
TGA		Reactivity; limited information on composition of organic and inorganic compounds	H_2O, aliphatics, aromatics, sugars, polymerized large hydrocarbons [40]	Aliphatics, acids, alkylphenols, oxygenated aromatics	Increase in sensitivity, simultaneous capture of product evaluation, broader ranges of compositional analysis [96]
Elemental		Organics	CHNOS	C: 60.8–72.7% db; O: 20.9–32.3% db. General remark: bio-oil has lower C (50–64% db) and higher O (35–40% db) than torrefaction tar	Systematic errors related to differences in calibration
KF titration	Methanol	H_2O	Total water content	Total water content	Systematic errors (Methanol used as a sample solvent may react with activated aldehyde/ketone groups present in the oils, and release water) [97]
Ion chromatography	Hydrolysis	Organic and halogens	Sugars and sugar degradation products (e.g. furans and organic acids), uronic acids, Cl, S [98]	Glucose	Decrease acquisition time for chromatographic run (approx. 30 min)
^{1}H-^{13}C NMR	Chloroform/ acetone	Organics	Hydroxyl groups, carbonyl groups, aromatic carbon, aliphatic carbon, heteroatoms containing bonds, sugars	Carboxylic acid, aldehydes, aromatics/ alkenes, ethers/ methoxy groups, aliphatics	Overlapping spectra for sugar-based and lignin-derived compounds, limited information on heavy molecular compounds, no information on individual components
Two-step Soxhlet extractor	Water - ethanol	Extractives	Water- and ethanol soluble material	No attempts to differentiate nitrogenous, inorganic and non-structured sugars	Need to develop new methods to analysis e.g. large, polymerized hydrocarbons, etc.
ESI-MS	Methanol	Organics			Separation efficiency, sensitivity for complex samples, information on low/ intermediate molecular size compounds (200–1000 Da) [99]
GC-FID	Methanol	Organics	Acids and ester content [100]	Acids, ester and derivatives: hexadecenoic acid, oleic, linoic, fatty	Separation efficiency, sensitivity for complex samples, information on the low molecular compounds (50–500 Da) [101]
UVvis	Methanol	Organics	Aromatics	Phenols and derivatives	Erroneous readings: UVvis does not differentiate between the sample of interest and contaminants that absorb at the same wavelength, limited to low molecular compounds (50–500 Da) [102]
HS GC–MS		Organics	Alkanes, aromatics, PAHs, nitrogenated organics and sulfur-containing organics	Aliphatics, small aromatics e.g. vanillin, cresols, including nitrogen-containing species	Separation efficiency, low molecular compounds (40–500 Da) [103]
ESI / APPI FT-ICR MS	DMSO	Organics	Identification of molecular species within a wide range of MW (200–1000 Da) with high mass resolution (better than 0.003 Da) [16]	Furfural derivatives, phenolics, aliphatics, oligomers, condensed aromatics and different size PAHs, sulphur and nitrogen-containing species	Instrumental and operational cost

3.3.4. Rheology

Figure 6 shows the temperature-dependent viscosity of the torrefaction tar, corn-based starch binder, cellulose and glycerol. Generally, tar and bio-oil are Newtonian fluids and do not show hysteresis. Glycerol, liquid tar and corn-based binder showed qualitatively similar viscosities that varied from 2.4 to 2.6 Pa s which remained constant through the entire experiment. The viscosity of liquid tar was almost 200 and 100 times greater than that of bio-oil and water-wood slurry, reported in previous studies [91,92]. The dynamic viscosity of cellulose decreased from 14 to 9 Pa s with increasing temperature from 50 to 80 °C. The viscosity of cellulose is similar to that of corn sillage both of which are non-Newtonian fluids [93–95]. The viscosity of liquid tar and corn-based starch binder was similar indicating that the liquid fraction collected from the torrefaction process could be successfully used as a binder for woodstove biomass briquetting.

4. Discussion

Chemical analysis of the liquid torrefaction tar showed that it consists of a complex mixture of light and heavy molecular weight compounds. The best solubility of tar was achieved in DMSO, acetone, DCM and chloroform which were used as solvents during qualitative FT-ICR and ^{1}H-^{13}C HS-QC NMR analysis. Based solely on the strong effect of solvents on the compositional analysis it might be expected that the tar structure is too complex to be analysed. However, results from the present work demonstrate that accurate prediction of the tar structure strongly depends on using several different but complementary analytical techniques.

All techniques used in the compositional characterisation of tar samples are summarized in Table 4. Overall, aliphatic and aromatic protons were more prevalent in both liquid and concentrated tar samples than alcohols and carbohydrates. The HSGC-MS analysis, direct injection GC–MS and GC-FID, UV-Fluorescence analysis indicated the presence of lipids, acids i.e. hexadecenoic, oleic, linoleic, phenols i,e, mono, di-tri-, and tetra-phenols, benzenoids and imidazoles. The results using FT-ICR MS showed that the liquid tar comprise of aromatic and aliphatic compounds which most likely include oxygen heteroatoms ranging from O_5 to O_9, nitrogen heteroatoms ranging from NO to N_2O_9 and sulfur heteroatoms varying from SO to S_3O_7.

The low ash content in the liquid tar indicated that nitrogen and sulphur were probably organically bound to the tar structure. The inorganic compounds in raw olive stones could either vaporize during torrefaction or remain in the char. Interestingly, no alkali metal compounds were detected in the liquid tar by FT-ICR MS and HSGC-MS analysis. FT-ICR analysis is an innovative way to characterise the complex composition of pyrolysis products.

For the first time, FT-ICR analysis was conducted on a liquid tar. The results showed that the torrefaction tar contains a high percentage of high molecular weight compounds. However, only comprehensive analysis of the tar structure using FT-ICR, NMR, UVvis and ion chromatography methods can provide information on compounds originating from different lignocellulosic fractions (cellulose, hemicellulose, lignin). The analytical limitations using all discussed techniques are referred to the absence of calibration standards to quantify the heavy molecular compounds. Overall, more research should be carried out to quantify the light and heavy molecular compounds in the liquid tar. The FT-ICR MS technique coupled to an ESI source ionization enables identification of polar and non-volatile compounds, such as sugars, proteins, and extractive derivatives. Moreover, the developed method using FT-ICR dynamic range of m/z can identify a broad spectrum of compounds which were difficult to detect with the other analytical techniques.

This work showed a great promise to use the FT-ICR technique in the characterisation of tar and bio-oil samples from high-temperature biomass treatment due to the high reproducibility, short analysis time and uncomplex data processing. The numbers of commercial vehicles increase every year requiring improvement of asphalt road facilities. For that reason, the road paving industry is interested in utilizing bio-based binder materials to improve the production, placement, and performance of asphalt mixtures. Thus, the volatile lean composition, low reactivity and high viscosity of the liquid tar are the most important properties for the use as a bio-based binder in biomass briquettes or as asphalt road pavement. In addition, low moisture content of less than 5.4 wt.% as received, the low ash content and its high calorific value of 26.1 MJ kg^{-1} will provide benefits for future uses of the liquid tar as a binding agent. The formation of solid tar condensate contained fewer oxygen-containing compounds and was less reactive in oxygen than liquid tar. These properties of tar could be perhaps considered beneficial for storage and transportation of tar. This result clearly demonstrates that tars as a by-product of the torrefaction process at Arigna Fuels could be a valuable feedstock for use as a bio-based binder in temperature-critical processes.

5. Conclusion

The combination of IC, GC–MS, ESI MS, GC-FID, UV-Fluorescence, TGA, HS-GC–MS and FT-ICR MS techniques provided comprehensive characterisation of tar samples from the pilot plant torrefaction of olive stones. To the best of our knowledge, this work is the first comparison of different analytical techniques for the characterisation of tars produced from torrefaction. The results of this study revealed that only the utilisation of a range of complementary analytical techniques can provide information on light and heavy molecular tar fractions, allowing the detection and characterisation of carbohydrates, phenolic and poly-aromatic compounds. The torrefaction tar viscosity was like that of fossil-based resin binders which were in general 100–200 times higher than that of bio-oil samples. The presence of organically bound sulphur and nitrogen detected with FT-ICR might limit the use of torrefaction tar as a fuel due to the potential formation of toxic emissions when combusted.

Declaration of Competing Interest

The authors declare that they have no known competing financial interests or personal relationships that could have appeared to influence the work reported in this paper.

Acknowledgements

Appendix A. Supplementary data

Supplementary data associated with this article can be found, in the online version, at https://doi.org/10.1016/j.fuel.2020.120086.

References

[1] Nättorp A, Dinkel F, Zschokke M. Environmental impact of biogenic oils as raw materials in road construction. Int J Pav Eng 2019;20:1–10.

[2] Riva L, Nielsen HK, Wang L, Bartocci P, Barbanera M, Bidini G. Analysis of optimal temperature, pressure and binder quantity for the production of biocarbon pellet to be used as a substitute for coke. Appl Energy 2020;256: 113933.

[3] Trubetskaya A, Hunt AJ, Budarin VL, Attard TM, Forsberg F, Arshadi M, et al. The effect of wood composition and supercritical CO_2 extraction on charcoal production in ferroalloy industries. Energy 2019;193:116696.

[4] Zeng Xi, Ueki Y, Yoshiie R, Naruse I, Wang F, Han Z and etc., Recent progress in tar removal by char and the applications: A comprehensive analysis, Carbon Res Conv (3) (2020) 1–18.

[5] Kujawinski EB, Hatcher PG, Freitas MA. High-resolution fourier transform ion cyclotron resonance mass spectrometry of humic and fulvic acids: improvements and comparisons. Anal Chem 2002;74:413–9.

[6] Tumuluru JS, Sokhansanj S, Hess JR, Wright CT, Boardman RD. A review on biomass torrefaction process and product properties for energy applications. Ind Biotech 2011;7(5):384–401.

[7] Bergman PCA, Boersma AR, Zwart RWH, Kiel JHA, Torrefaction for biomass co-firing in existing coal-fired power stations, Report ECN-C-05-013 ECN (2005) 1–79.

[8] Umeki K, Bach-Oller A, Häggström G, Furusjö E. Reduction of tar and soot formation from entrained-flow gasification of woody biomass by alkali impregnation. Energy Fuels 2017;31(5):5104–10.

[9] Warnock AM, Hagen SC, Passeri DL. Marine tar residues: a review. Water Air Soil Pollut 2015;226(68):1–24.

[10] Prins MJ, Ptasinski KJ, Janssen FGGJ. Torrefaction of wood: Part 2, Analysis of products. J Anal Appl Pyrolysis 2006;77(1):35–40.

[11] Diaz C, Blanco CG. NMR: a powerful tool in the characterization of coal tar pitch. Energy Fuels 2003;17:907–13.

[12] Trubetskaya A, Souihi N, Umeki K. Categorization of tars from fast pyrolysis of pure lignocellulosic compounds at high temperature. Renew Energy 2019;141: 751–9.

[13] Wang Y, Liu Y, Wang W, Liu L, Hu C. Torrefaction at 200C of Pubescens Preated with AlCl3 Aqueous Solution at Room Temperature. ACS Omega 2020;5(42): 27709–22.

[14] Fetzer JC. The chemistry and analysis of large PAHs. Polycycl Arom Comp 2007; (27):143–62.

[15] Matsakas L, Gao Q, Jansson S, Rova U, Christakopoulos P. Green conversion of municipal solid wastes into fuels and chemicals. El J Biotech 2017;26:69–83.

[16] Stankovikj F, McDonald AG, Helms GL, Olarte MV, Garcia-Perez M. Characterization of the water-soluble fraction of woody biomass pyrolysis oils. Energy Fuels 2017;31(2):1650–64.

[17] Mullen CA, Strahan GD, Boateng AA. Characterization of various fast-pyrolysis bio-oils by NMR spectroscopy. Energy Fuels 2009;23:2707–18.

[18] Joseph J, Baker C, Mukkamala S, Beis SH, Clayton Wheeler M, et al. Chemical shifts and lifetimes for nuclear manetic resonance (NMR) analysis of biofuels. Energy Fuels 2010;24:5153–62.

[19] Stankovikj F, McDonald AG, Helms GL, Olarte MV, Garcia-Perez M. Quantification of bio-oil functional groups and evidences of the presence of pyrolytic humins. Energy Fuels 2016;30(8):6505–24.

[20] Horvat A, Kwapinska M, Xue G, Dooley S, Leahy JJ. Detailed measurement uncertainty analysis of solid-phase adsorption – total gas chromatography (GC)-detectable tar from biomass gasification. Energy Fuels 2016;30(3):2187–97.

[21] Jarrell TM, Marcum CL, Sheng H, Owen BC, O'Lenick CJ, Maraun H, et al. Characterization of organosolv switchgrass lignin by using high performance liquid chromatography/high resolution tandem mass spectrometry using hydroxide-doped negative-ion mode electrospray ionization. Green Chem 2014; 16:2713–27.

[22] D'Auria M, Emanuele L, Racioppi R. FT-ICR-MS analysis of lignin. Nat Prod Res 2012;26(15):1368–74.

[23] Qi Y, Volmer DA. Rapid mass spectral fingerprinting of complex mixtures of decomposed lignin: data-processing methods for high-resolution full-scan mass spectra. Rapid Commun Mass Spectrom 2018;33(S1):2–10.

[24] Hertzog J, Carre V, Brech YL, Dufour A. Towards controlled ionization conditions for ESI-FT-ICR-MS analysis of bio-oils from lignocellulosic material. Energy Fuels 2016;30(7):5729–39.

[25] Echavarri-Bravo V, Tinzl M, Kew W, Cruickshank F, Logan Mackay C, Clarke DJ, Horsfall LE. High Resolution Fourier Transform Ion Cyclotron Resonance Mass Spectrometry (FT-ICR MS) for the characterization of enzymatic processing of commercial lignin. New Biotech 2019;52:1–8.

[26] Nakanishi T, Okamoto N, Tanaka K, Shimizu A. Laser desorption time-of-flight mass spectrometric analysis of transferrin precipitated with antiserum: a unique simple method to identify molecular weight variants. Biol Mass Spectrom 1994;4: 230–3.

[27] Solouki T, Gillig KJ, Russell DH. Detection of high-mass biomolecules in Fourier transform ion cyclotron resonance mass spectrometry: theoretical and experimental investigations. Anal Chem 1994;66(9):1583–7.

[28] Solouki T, Emmett MR, Guan S, Marshall AG. Detection, number, and sequence location of sulfur-containing amino acids and disulfide bridges in peptides by ultrahigh-resolution MALDI FTICR mass spectrometry. Anal Chem 1997;69(6): 1163–8.

[29] Trubetskaya A, Leahy JJ, Grams J, Kwapinska M, Johnson R, Monaghan RFD, et al. The effect of particle size, temperature and residence time on the yields and reactivity of olive stones from torrefaction. Renew Energy 2020;160:998–1011.

[30] Trubetskaya A, Leahy JJ, Yazhenskikh E, Layden P, Johnson R, Monaghan RFD, et al. Characterization of woodstove briquettes from torrefied biomass and coal. Energy 2019;171:853–65.

[31] Sluiter A, Hames B, Ruiz R, Scarlata C, Sluiter J, Templeton D, et al. Determination of structural carbohydrates and lignin in biomass. Report NREL/TP-510-42618 2008:1–18.

[32] Guillen MD, Blanco J, Canga JS, Blanco CG. Study of the effectiveness of 27 organic solvents in the extraction of coal tar pitches. Energy Fuels 1991;5: 188–92.

[33] Zhang W, Andersson JT, Räder HJ, Müllen K. Molecular characterization of large polycyclic aromatic hydrocarbons in solid petroleum pitch and coal tar pitch by high resolution MALDI ToF MS and insights from ion mobility separation. Carbon 2015;95:672–80.

[34] Osman NB, McDonald AG, Laborie MPG, Adhikari S. Analysis of DCM extractable components from hot-pressed hybrid poplar. Holzforschung 2012;66:927–34.

[35] MS-SEARCH, NIST Mass Spectrometry Data Center: NIST/EPA/NIH Mass Spectral Database, http://chemdata.nist.gov.

[36] Garcia A, Culebras M, Collins MN, Leahy JJ. Stability and rheological study of sodium carboxymethyl cellulose and alginate suspensions as binders for lithium ion batteries. Appl Pol Sci 2018;135(17):1–6.

[37] Johnson R, Hydrothermal processing of biomass and related model compounds [Ph.D. thesis], University of Leeds; 2012.

[38] Tumuluru JS. Effect of deep drying and torrefaction temperature on proximate, ultimate composition, and heating value of 2-mm lodgepole pine (pinus contorta) grind. Bioengineering 2016;3(16):1–18.

[39] Yu Y, Chua YW, Wu H. Characterization of pyrolytic sugars in bio-oil produced from biomass. Energy Fuels 2012;30:4145–9.

[40] Trubetskaya A, Lange H, Wittgens B, Brunsvik A, Crestini C, Rova U, et al. Structural and thermal characterization of novel organosolv lignins from wood and herbaceous sources. Processes 2010;8(7):1–21.

[41] Kanaujia PK, Production, Upgrading and Analysis of Bio-oils Derived from Lignocellulosic Biomass, Polysaccharides (2014) 1–26.

[42] Theander O. Chemical analysis of lignocellulosic materials. Animal Feed Sci Tech 1991;32:35–44.

[43] Yu H, Zhang Z, Li Z, Chen D. Characteristics of tar formation during cellulose, hemicellulose and lignin gasification. Fuel 2014;118:250–6.

[44] Yang H, Yan R, Chen H, Lee DH, Zheng C. Characteristics of hemicellulose, cellulose and lignin pyrolysis. Fuel 2007;86:1781–8.

[45] Dudynski M, van Dyk JC, Kwiatkowski K, Sosnowska M. Biomass gasification: influence of torrefaction on syngas production and tar formation. Fuel Process Tech 2015;131:203–12.

[46] Sima-Ella E, Yuan G, Mays T. A simple kinetic analysis to determine the intrinsic reactivity of coal chars. Fuel 2005;84(14–15):1920–5.

[47] Bassilakis R, Carangelo RM, Wojtowicz MA. TG-FTIR analysis of biomass pyrolysis. Fuel 2001;80:1765–86.

[48] Wilson MA, Hatcher PG. Detection of tannins in modern and fossil barks and in plant residues by high resolution solid-state 13C nuclear magnetic resonance. Org Geochem 1988;12:539–46.

[49] Salami A, Vilppo T, Weisell J, Raninen K, Pitkänen S, Lappalainen R. Cost-effective FTIR and ^{1}H NMR spectrometry used to screen valuable molecules extracted from selected West African trees by a sustainable biochar process. Sci African 2020;8:1–13.

[50] Undri A, Abou-Zahid M, Briens C, Berruti F, Rosi L, Frediani M, et al. A simple procedure for chromatographic analysis of biool from pyrolysis. J Anal Appl Pyrolysis 2015;114:208–21.

[51] Vlahov G. Quantitative 13C NMR method using DEPT pulse sequence for the detection of olive oil adulteration with soybean oil. NMR Food Sci 1998;35(13): 8–12.

[52] Matuszwska A, Czaja M. The use of synchronous luminescence spectroscopy in qualitative analysis of aromatic fraction of hard coal thermolysis product. Talanta 2000;52:457–64.

[53] Rapagna S, Gallucci K, Di Marcello M, Matt M, Foscolo PU, Nacken M, et al. Characterisation of tar produced in the gasification of biomass with in situ catalytic reforming. Int J Chem Reac Eng 2010;8(A30):1–14.

[54] Li CZ, Wu F, Cai HY, Kandiyoti R. UV-fluorescence spectroscopy of coal pyrolysis tars. Energy Fuels 1994;8(5):1039–44.

[55] Morgan TJ, Millan M, Behrouzi M, Herod AA, Kandiyoti R. On the limitations of UV-fluorescence spectroscopy in the detection of high-mass hydrocarbon molecules. Energy Fuels 2005;19(1):164–9.

[56] Gonzalez-Vila FJ, Tinoco P, Almendros G, Martin F. Pyrolysis-GC-MS analysis of the formation and degradation stages of charred residues from lignocellulosic biomass. J Agricult Food Chem 2001;49(3):1128–31.

[57] Ghorbannezhad P, Firouzabadi MD, Ghasemian A. Catalytic fast pyrolysis of sufarcane bagasse pith with HZSM-5 catalyst using tandem micro-reactor-GC-MS. Energy Sour, Part A: Rec, Util, Env Effects 2018;40(1):15–21.

[58] Yoshikawa T, Shinohara S, Yagi T, Ryumon N, Nakasaka Y, Tago T, et al. Production of phenols from lignin-derived slurry liquid using iron oxide catalyst. Appl Catal B Environ 2014;146:289–97.

[59] Hao N, Ben H, Yoo CG, Adhikari S, Ragauskas AJ. Review of NMR characterization of pyrolysis oils. Energy Fuels 2016;30(9):6863–80.

[60] Wei L, Liang S, Guho NM, Garcia-Perez M, McDonald AG, Hanson AJ, et al. Production and characterization of bio-oil and biochar from the pyrolysis of residual bacterial biomass from a polyhydroxyalkanoate production process. J Anal Appl Pyrolysis 2015;115:268–78.

[61] Waggoner DC, Wozniak AS, Cory RM, Hatcher PG. The role of reactive oxygen species in the degradation of lignin derived dissolved organic matter. Geochimica at Cosm Acta 2017;208:171–84.

[62] Huba AK, Gardinali PR. Characterization of a crude oil weathering series by ultrahigh-resolution mass spectrometry using multiple ionization modes. Sci Total Environ 2016;563–564:600–10.

[63] Zheng Q, Morimoto M, Sato H, Fouquet T. Resolution-enhanced Kendrick mass defect plots for the data processing of mass spectra from wood and coal hydrothermal extracts. Fuel 2019;235:944–53.

[64] Hsu CS, Qian K, Chen YC. An innovative approach to data analysis in hydrocarbon characterization by on-line liquid chromatography-mass spectrometry. Anal Chim Actra 1992;264:79–89.

[65] Wilson RM, Tfaily MM. Advanced molecular techniques provide new rigorous tools for characterizing organic matter quality in complex systems. JGR Biogeosci 2018;123(6):1790–5.

[66] Jeong HJ, Cha JY, Choi JH, Jang KS, Lim J, Kim WY, et al. One-pot transformation of technical lignins into humic-like plant stimulants through fenton-based advanced oxidation: accelerating natural fungus-driven humification. ACS OMEGA 2018;3:7441–53.

[67] Qi Y, Fu P, Li S, Ma C, Liu C, Volmer DA. Assessment of molecular diversity of lignin products by various ionization techniques and high-resolution mass spectrometry. Sci Tot Env 2020;713:1–8.

[68] Zander M, Haenel MW. Regularities in the fluorescence spectra of coal-tar pitch fractions. Fuel 1990;69:1206–7.

[69] Morgan TJ, Kandiyoti R. Pyrolysis of coals and biomass: analysis of thermal breakdown and its products. Chem Rev 2014;114:1547–607.

[70] Cole DP, Smith EA, Lee YJ. High-resolution mass spectrometric characterization of molecules on biochar from pyrolysis and gasification of switchgrass. Energy Fuels 2012;26:3803–9.

[71] Schaub TM, Hendrickson CL, Quinn JP, Rodgers RP, Marshall AG. Instrumentation and method for ultrahigh resolution field desorption ionization fourier transform ion cyclotron resonance mass spectrometry of nonpolar species. Anal Chem 2005;77(5):1317–24.

[72] Leonardis I, Chiaberge S, Fiorani T, Spera S, Battistel E, Bosetti A, et al. Characterization of Bio-oil from Hydrothermal Liquefaction of Organic Waste by NMR Spectroscopy and FTICR Mass Spectrometry. CHEMSUSCHEM 2013;6: 160–7.

[73] Wu Z, Rodgers RP, Marshall AG. Characterization of vegetable oils: detailed compositional fingerprints derived from electrospray iinozation fourier transform ion cyclotron resonance mass spectrometry. J Agri Food Chem 2004;52:5322–8.

[74] Meesuk S, Cao JP, Sato K, Hoshino A, Utsumi K, Takarada T. Nitrogen conversion of pig compost during pyrolysis. J Chem Eng Japan 2013;46(8):556–61.

[75] Snyder LR. Column efficiency in liquid-solid adsorption chromatography. H.E.T. P. [height equivalent to a theoretical plate] values as a function of separation conditions. Anal Chem 1967;39(7):698–704.

[76] Snyder LR, Buell BE, Howard HE. Nitrogen and oxygen compound types in petroleum. Total analysis of a 700–850F disillate from a California crude oil. Anal Chem 1968;40(8):1303–17.

[77] Jarvis JM, Billing JM, Hallen RT, Schmidt AJ, Schaub TM. Hydrothermal liquefaction biocrude compositions compared to petroleum crude and shale oil. Energy Fuels 2017;31(3):2896–906.

[78] Marshall AG, Rodgers RP. Petroleomics: the next grand challenge for chemical analysis. Acc Chem Res 2004;37(1):53–9.

[79] Saleh SB, Flensborg JP, Shoulaifar TK, Sarossy Z, Hansen BB, Egsgaard H, et al. Release of chlorine and sulfur during biomass torrefaction and pyrolysis. Energy Fuels 2014;28:3738–46.

[80] Rennenberg H, Brunold CH, De Kok L, Stulen I. Sulfur nutrition and sulfur assimilation in higher plants. SPB Academic Publishing 1990.

[81] Dayton DC, Belle-Oudry D, Nordin A. Effect of coal minerals on chlorine and alkali metals released during biomass/coal firing. Energy Fuels 1999;13:1203–11.

[82] Zhang J, Qian C, Jiang B. Characterization of bio-crude from hydrothermal liquefaction of Enteromorpha prolifera by FT-ICR mass spectrometry. Energy Procedia 2017;142:172–6.

[83] Smith EA, Park S, Klein AT, Lee YJ. Bio-oil analysis using negative electrospray ionization: comparative study of high-resolution mass spectrometers and phenolic versus sugaric components. Energy Fuels 2015;26(6):3796–802.

[84] Tessarolo NS, Silva RC, Vanini G, Pinho A, Romao W, Azevedo DA, et al. Assessing the chemical composition of bio-oils using FT-ICR mass spectrometry and comprehensive two-dimensional gas chromatography with time-of-flight mass spectrometry. Microchem J 2014;117:68–76.

[85] Smith EA, Thompson C, Lee YJ. Petroleomic characterization of bio-oil aging using fourier-transform ion cyclotron resonance mass spectrometry. Bull Korean Chem Soc 2014;35(3):811–4.

[86] Kekäläinen T, Venäläinen T, Jänis J. Characterization of birch wood pyrolysis oils by ultrahigh-resolution fourier transform ion cyclotron resonance mass spectrometry: insights into thermochemical conversion. Energy Fuels 2014;28: 4596–602.

[87] Barker D. Lignans. Molecules 2016;24:1424.

[88] Patwardhan PR, Brown RC, Shanks BH. Understanding the fast pyrolysis of lignin. ChemSusChem 2011;4(11):1629–36.

[89] Hiltunen E, Pakkanen TT, Alvila L. Phenolic extractives from wood of birch (Betula pendula). Holzforschung 2004;58:326–9.

[90] Wang L, Li X, Wang Z. Whole body radioprotective effect of phenolic extracts from the fruits of Malus baccata (Linn) Borkh. Food Func 2016;7(2):975–81.

[91] Nolte MW, Liberatore MW. Viscosity of biomass pyrolysis oils from various feedstocks. Energy Fuels 2010;24:6601–8.

[92] He W, Park CS, Norbeck JM. Rheological study of comingled biomass and coal slurries with hydrothermal pretreatment. Energy Fuels 2009;23:4763–7.

[93] Conti F, Wiedemann L, Sonnleitner M, Goldbrunner M. Thermal behaviour of viscosity of aqueous cellulose solutions to emulate biomass in anaerobic digesters. New J Chem 2018;42:1099–104.

[94] Wiedemann L, Conti F, Sonnleitner M, Janus T, Zörner W, Goldbrunner M. Mixing in biogas digesters and development of an artificial substrate for laboratory-scale mixing optimization. Chem Eng Tech 2017;40(2):238–47.

[95] Brehmer M, Eppinger T, Kraume M. Einfluess der Rheologie auf das Strömungsregime in gerührten grosstechnischen Biogasreaktoren. Chemie Ing Tech 2012;84(11):2048–56.

[96] Loof D, Hiller M, Oschkinat H, Koschek K. Quantitative and qualitative analysis of surface modified cellulose utilizing TGA-MS. Materials 2016;9(6):1–14.

[97] Chum H. Biomass pyrolysis oil feedstocks for phenolic adhesives. In: Hemingway RW, Conner AH, Branham SJ, editors. Adhesives from renewable resources. American Chemical Society; 1989. p. 135–51.

[98] Hayes DJM. Development of near infrared spectroscopy models for the quantitative prediction of the lignocellulosic components of wet Miscanthus samples. Biores Tech 2012;119:393–405.

[99] Alsbou E, Helleur B. Direct infusion mass spectrometric analysis of bio-oil using ESI-ion-trap MS. Energy Fuels 2014;(28):578–90.

[100] Michailof CM, Kalogiannis KG, Sfetsas T, Patiaka DT, Lappas AA. Advanced analytical techniques for bio-oil characterization. John Wiley Sons 2016;5(6): 1–26.

[101] Lu Y, Li GS, Lu YC, Fan X, Wei XY. Analytical strategies involved in the detailed componental characterization of biooil produced from lignocellulosic biomass. Int J Anal Chem 2017:1–19.

[102] Samburova V, Zenobi R, Kalberer M. Characterization of high molecular weight compounds in urban atmospheric particles. Atmos Chem Phys 2005;(5):2163–70.

[103] Wong YF, Yan DD, Shellie RA, Sciarrone D, Marriott PJ, Rapid Plant Volatiles Screening Using Headspace SPME and Person-Portable Gas Chromatography-Mass Spectrometry, Chromatog (82) (2018) 297–305.